ScieRxiv
NOT PEER-REVIEWED
Review

Advancements in physical metallurgy- guided machine learning for predicting continuous cooling phase transformations in steels: A comprehensive review

Rui Han[1,2], Wentao Zhao[1], Juan Yang[1], Yaru Wang[1], He Yang[1], Xiaoxu Huang[1,2], Ziyong Hou[1,2,3*]

[1]International Joint Laboratory for Light Alloys (Ministry of Education), College of Materials Science and Engineering, Chongqing University, Chongqing 400044, China.
[2]State Key Laboratory of Mechanical Transmission for Advanced Equipment, Chongqing University, Chongqing 400044, China.
[3]Institute of Frontier Interdisciplinary Studies, Chongqing University, Chongqing 400044, China.

***Correspondence to:** Prof. Ziyong Hou, International Joint Laboratory for Light Alloys (Ministry of Education), College of Materials Science and Engineering, Chongqing University, Chongqing 400044, China. E-mail: houzy@cqu.edu.cn

Received: 10 May 2026 | Approved: 22 May 2026 | Online: 22 May 2026

Abstract

The rapid advancement of artificial intelligence (AI) and the exponential growth of material big data have created exciting opportunities for applying machine learning (ML) in materials science. By harnessing this big data, ML enables the discovery of complex structure-property relationships, offering a pathway to accelerate materials design while reducing experimental costs. This paradigm is particularly impactful for Material Genetic Engineering (MGE) and the data-driven development of advanced high-strength steels. Central to alloys and heat treatment optimization in steels is the

continuous cooling transformation (CCT) diagram. Experimentally constructing CCT diagrams remains labor-intensive and requires deep domain expertise, whereas conventional physics-based models are often limited in accuracy and generalizability. This review critically examines the application of ML methods in predicting CCT diagrams, comparing their performance with traditional physical metallurgy (PM) approaches. Particular attention is given to the limitations of purely data-driven methods, especially in capturing complex thermomechanical phenomena such as hot deformation, and the emerging trend toward hybrid modeling strategies that integrate PM principles. Such synergistic frameworks are expected to enhance predictive robustness and accelerate the rational design of next-generation steels.

Keywords: Steels, machine learning, continuous cooling transformation, hot deformation, physical metallurgy

INTRODUCTION

Steel constitutes a cornerstone of global manufacturing and infrastructure. While annual production has surpassed 1.8 billion tons, led by major producers such as China, India, and the United States, the industry faces mounting pressures, including overcapacity, trade tariffs, and the transition toward low-carbon technologies[1,2]. While rigorous testing of microstructures and mechanical properties is essential for productivity gains, these processes can also introduce inefficiencies. Conventional alloy design remains heavily reliant on empirical trial-and-error methods, which extend research timelines. Consequently, achieving carbon neutrality without compromising productivity is a critical challenge[3-5].

Steels are fundamental to engineering and structural applications, with their mechanical performance governed by the interplay between chemical composition and microstructure. During continuous cooling, undercooled austenite undergoes a series of phase transformations that dictate final properties, making the interpretation of CCT diagrams crucial for heat treatment optimization[6]. These CCT diagrams offer quantitative insights into phase transformation temperatures over a range of cooling

rates and are affected by factors such as chemical composition, cooling rate, prior austenite grain size, austenitizing conditions, temperature and holding time, as well as other processing parameters[7]. The primary experimental techniques for constructing CCT diagrams, such as metallography, hardness testing, and dilatometry[8], are often labor-intensive, costly, and require specialized expertise. Consequently, there is a compelling need for more efficient and accessible methodologies to determine CCT diagrams and further understanding of phase transformation behavior in steels[9], as shown in Figure 1.

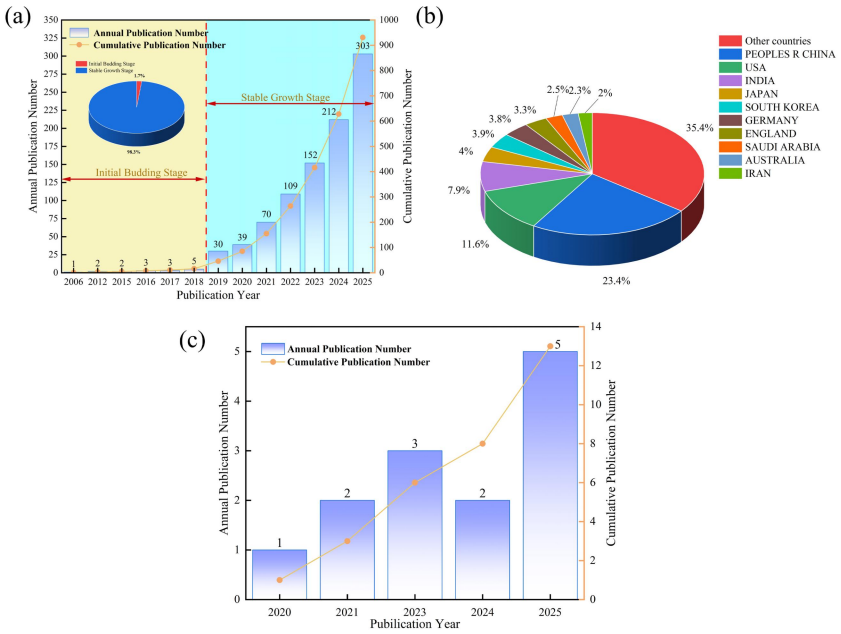

Figure 1. (A) Bibliometric analysis of ML applications in steels, highlighting annual and cumulative publication numbers from 2006 to 2025; (B) Geographic distribution of publications on AI in steels, based on data from the Web of Science Core Collection; (C) Research trends in phase transformation prediction in steels, with particular emphasis on CCT diagrams and deformation parameters.

PM has established robust mathematical models for phase transformation mechanisms[10-12], flow stress[13,14], and recrystallization[15,16]. enable systematic exploration of the intricate links between composition, processing, microstructure, and mechanical properties in steels. While traditional mathematical models continue to

provide valuable insight into microstructures evolution and mechanical properties in steels, their utility can be limited by the increasingly complex and data-rich environment of the modern steel industry. Commercial software like Thermo-Calc and JMatPro predicts CCT diagrams via thermodynamics or semi-empirical modeling approaches, yet often falls short in capturing real-world variables such as hot deformation and strain rate[9].

To address the challenges posed by materials big data, traditional approaches in materials science are being reevaluated. Concepts such as MGE, Integrated Computational Materials Engineering (ICME), and ML have emerged[17] as powerful tools for cost-effective, efficient data analysis. This data-driven approach holds the potential to revolutionize the prediction capabilities within materials science by leveraging existing data to inform future research directions[18]. Figure 2 outlines the evolution of phase transformation models from classical theory to data-driven fusion[20-31].

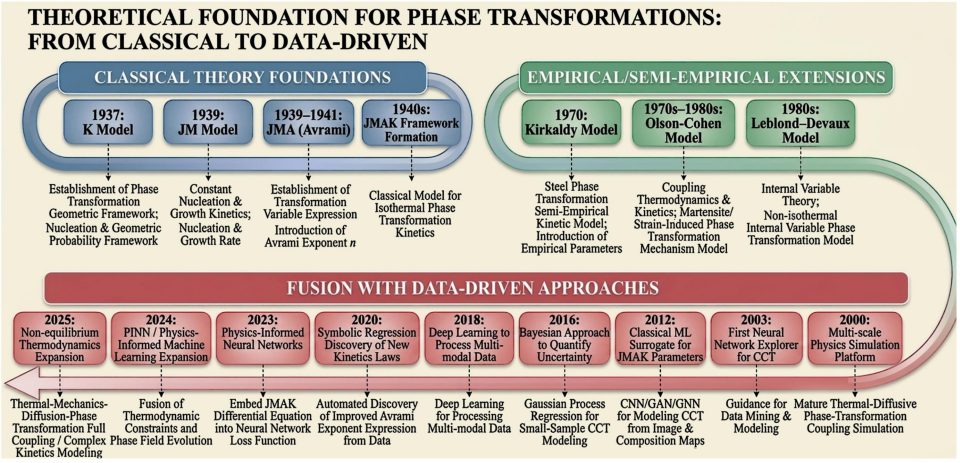

Figure 2. Evolution of phase transformation kinetics models from classical theory to data-driven fusion. Reproduced with permission[19-30].

Thus, this study aims to provide a comprehensive review of the application of PM models for predicting CCT diagram in steel. It will also discuss the contribution of ML models to steel design and optimization, and summarizes recent progress in integrating

ML with PM models for CCT diagram prediction. Finally, we explore future perspectives regarding the integration of physical principles into ML frameworks to guide the design of next-generation steels.

PREDICTING CONTINUOUS COOLING TRANSFORMATION IN PHYSICAL METALLURGICAL MODELING

A fundamental challenge in steel design lies in the accurate prediction of microstructure and mechanical properties. This predictive capability is central not only to the optimization of chemical composition but also to the design of thermos-mechanical treatments for industrial applications. A key step in this endeavor is the construction of the CCT and time-temperature-transformation (TTT) curves, as illustrated in Figure 3.

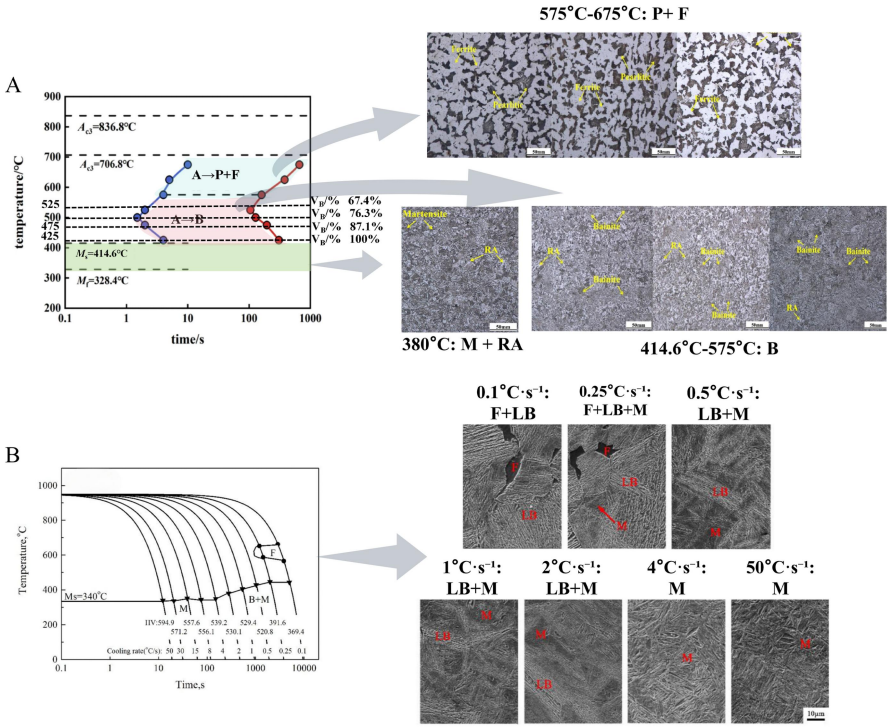

Figure 3. Overview of phase transformation in steels: (A) CCT curve and corresponding microstructure. Copyright 2019, Wiley-VCH GmbH, Reproduced with permission[31]; (B) TTT diagram and corresponding isothermal microstructure. Copyright 2025, Springer Nature, Reproduced with permission[32]. A_{c3}: Austenitization Start Temperature; M_s: Martensite Start Temperature; M_f: Martensite Finish Temperature; P: Pearlite; F: Ferrite; M: Martensite; RA: Retained Austenite; B: Bainite;

LB: Lath Bainite.

Since the 1940s, the Johnson-Mehl-Avrami-Kolmogorov (JMAK) model has served as a foundational framework for describing the kinetics of isothermal, diffusion-controlled phase transformations[33-35]. The core of the JMAK model is encapsulated in Eq. (1):

$$X = 1 - \exp(-k \cdot t^n) \qquad (1)$$

Where X represents the volume fraction of the phase, k is a temperature-dependent constant, t denotes the time elapsed during phase transformation, and n is a constant determined by the transformation mechanism. In industrial applications, the dynamic transformation behavior under continuous cooling is of greater relevance than under isothermal condition. Therefore, predicting the phase transformation of steel during continuous cooling based on isothermal data has become a critical research topic[36]. To extend the JMAK formalism to non-isothermal conditions, the Scheil Additivity Rule, as presented in Eq. (2), is commonly employed[35,37,38].

$$\sum_{i=1}^{n} \frac{\Delta t_i}{\tau_i} = 1 \qquad (2)$$

Where Δt_i is the isothermal time at a given temperature, and τ_i is the incubation period at that temperature. However, this approach is computationally intensive, limiting its broad applicability. Consequently, since the 1970s, efforts have shifted toward developing explicit models for continuous cooling. Kirkaldy and Venugopalan (K-V)[39] pioneered a semi-empirical mathematical model grounded in PM principles.

Subsequent research has refined the K-V model by integrating nucleation, growth, and thermodynamic theories, resulting in more rigorous and comprehensive descriptions of phase transformation, especially under variable cooling conditions. For the diffusionless

transformations from austenite to martensite, the Koistinen-Marburger (K-M) model is widely adopted to quantify martensite kinetics, expressing the transformed fraction as a function of temperature with improved accuracy and predictive capability, as shown in Eq. (3)[40,41].

$$X_M = X_A \cdot \left\{1 - \exp\left[-\alpha\left(M_s - T\right)\right]\right\} \quad (3)$$

Where X_M denotes the volume fraction of martensite, X_A is the volume fraction of austenite available for transformation, α is the material-dependent constant, M_s indicates the martensite starting temperature, and T is the current temperature.

Based on these previous studies, numerous studies have sought to reconstruct and refine models to enhance the accuracy and generalizability of phase transition simulations. For example, Umemoto *et al.*[42] and Lee *et al.*[43] incorporated sublattice models to predict transformation kinetics and precipitation behavior in HSLA steels. Pei *et al.*[11] established regression models correlating transformation temperatures and fractions with cooling rates, demonstrating strong agreement with experimental data. Finite element method (FEM) implementations have further extended these models. Chen *et al.*[35] investigated the JMAK and K-M models into ABAQUS, confirming that accounting for incubation time improves the prediction of temperature-phase coupling. Similarly, Zhao *et al.*[33] adapted these frameworks for hot-stamping processes, validating them against Jominy end-quench tests.

Collins *et al.*[41] advanced the modified K-V model[44], which integrates Zener-Hillert kinetic growth and Cahn site saturation models, by incorporating a carbon-partitioning model, thermodynamic boundary conditions, and the K-M model. This comprehensive approach enabled more accurate prediction of CCT behavior in HSLA steels, as confirmed by experimental validation. Building on this, Zhang *et al.*[45] established a kinetic model for austenitization in Cr-Ni-Mo-V steel, demonstrating that diffusion is

the primary mechanism of austenite transformation. Additionally, a kinetic model for bainite transformation was developed using the J-M-A model, elucidating the nucleation sites and grain growth mechanisms of bainite, and simulated martensitic transformation kinetics via the K-M model. Saunders *et al.*[46] designed a model for TTT and CCT diagrams calculation based on the Kirkaldy model, which has been implemented in the JMatPro software. Martin *et al.*[47] introduced a model that incorporates the interactive effects of alloying elements during transformation, providing quantitative analysis and validation for their combined impact on CCT diagram predictions.

However, a significant limitation of these classical models is the neglect of thermomechanical processing. In industrial production, deformation in the austenite non-recrystallization region significantly accelerates transformation kinetics[42]. To address this, Xu *et al.*[48] combined the superelement model, Cahn nucleation theory[49], and the Scheil rule to establish a robust computational framework for predicting phase transformation kinetics and constructing CCT diagrams in low-carbon Nb steel, explicitly incorporating the influence of strain on supercooling, which demonstrated its accuracy and practical applicability through excellent agreement between model predictions and experimental data. Pohjonen *et al.*[50] developed a computational model to predict phase transformation start temperatures under various cooling paths, systematically evaluating the effects of alloying elements and strain. In a parallel study, Pohjonen *et al.*[12] employed the JMAK model to fit continuous cooling data for steel subjected to two different deformation conditions, with particular emphasis on the impact of deformation below the recrystallization temperature on phase transformation kinetics. Aranas *et al.*[51] proposed a novel approach for determining the critical stress required for dynamic transformation in steel, based on the free-energy difference between austenite and ferrite and the yield strength of newly formed ferrite. This methodology enables accurate simulation of dynamic transformation above the Ae_3 temperature during thermomechanical processing, substantially reducing dependence on resource-intensive hot-deformation experiments. Table 1 provides an overview of major phase transformation models in the literature, emphasizing their importance in

improving the accuracy and efficiency of simulating continuous-cooling phase transformations and constructing CCT diagrams for steel.

Despite these advancements, conventional PM models often suffer from limited generalizability across diverse steel grades due to scarcity of high-quality thermodynamic and kinetic data. This constraint hinders their direct application in the era of high-throughput materials design. Consequently, there is a growing impetus to develop data-driven methodologies that can capture complex, non-linear composition-processing-microstructure relationships beyond the reach of traditional physics-based models.

Table 1. Summary of the PM models for steels in literature.

Task	Model	Material	Reference
Phase transformation temperature	F_z=820.1−57.56ln (v_c+2.36) P_z=681.3−14.51ln (v_c−0.141) B_z=719.6−72.4ln (v_c+3.624) M_z=617.6−62.01ln (v_c+1.016)	Low carbon high strength sheet steel	[11]
Phase transformation volume fraction	F%=1− exp [−1.102(v_c−0.175)−0.0694] P%=1− exp [−0.4043(v_c−0.1908)0.0816] B%=1− exp [−21.94(v_c+44.24)−0.7582] M%=1− exp [−0.144(v_c−1.573)0.404]	Low carbon high strength sheet steel	[11]
Phase transformation volume fraction	$F=1-\exp[-b\left(\frac{D\gamma_{TTT}}{D\gamma}\right)^{m}(t-t_s)^{n}]$	22MnB5 steel	[52]

Phase transformation volume fraction	$X=X^{*}\cdot\left[1-W*\exp\left(-k\cdot\tau^{n}\right)-(1-W)*\exp$	High-strength steel	[53]
Isothermal incubation time	$\tau(X,T)=\frac{F(\mathrm{C,Mn,Si,Ni,Cr,Mo},G)}{\Delta T^{n}\exp\left(-\frac{\mathrm{Q}}{\mathrm{RT}}\right)}S(X)$ $S(X)=\int_{0}^{X}\frac{\mathrm{d}X}{X^{0.4(1-X)}(1-X)^{0.4X}}$	Low alloy steel	[54,55]
Phase transformation start temperature	$T_{\mathrm{f}}(t)=796.97-243.37\mathrm{C}-55.70\mathrm{Mn}+18.47\mathrm{Si}-53.91\mathrm{Ni}-22.72\mathrm{Mo}-15.30\mathrm{Cr}-4182.67\mathrm{B}+8.33\mathrm{Co}+63.05\mathrm{CNi}+9.56\,\mathrm{arcsinh}\left(t-t_{\mathrm{cr,f}}\right)$ $T_{\mathrm{b}}(t)=859.24-559.36\mathrm{C}-96.44\mathrm{Mn}+43.54\mathrm{Si}-45.95\mathrm{Ni}-120.91\mathrm{Mo}-87.87\mathrm{Cr}-24516\mathrm{B}+23.62\mathrm{Co}-99.71\mathrm{SiMo}-39.10\mathrm{NiMo}+74.87\,\mathrm{arcsinh}\left(\log_{10}\left(1+t-t_{\mathrm{cr,b}}\right)\right)$ $T_{m}=406.66-843.11\mathrm{C}+528.00\mathrm{Mn}-20.50\mathrm{Si}-20.79\mathrm{Ni}+20.55\mathrm{Mo}-19.51\mathrm{Cr}-250.93\mathrm{Mn}^{2}$	steels	[56]
Phase transformation volume fraction	$f_{B}=1-\exp\left(-2.52\times10^{-12}t^{3.12}\right)$ $f_{M}=1-\exp[f_0](-0.01035\ (337-T)^{1.229})$	Cr-Ni-Mo-V steel	[57]
Phase transformation volume fraction	$X_{\mathrm{F1}}=1-\exp\left(-\frac{\pi I_{\mathrm{s}}S_{\gamma}G_{\mathrm{F}}^{3}t^{4}}{3}\right)$ $X_{\mathrm{F2}}=1-\exp\left(-2S_{\gamma}G_{\mathrm{F}}t\right)$	Low carbon niobium steel	[58]
phase transformation start temperature	$T_{\mathrm{s,cct}}(\mathrm{K})=273.15+B_{0}+\sum_{i}B_{i}c_{i}+B_{t}\mathrm{arcsinh}\left(t_{85}-t_{85,\mathrm{k}}\right)$ $\log_{10}\left(t_{85,\mathrm{k}}\right)=A_{0}+\sum_{i}A_{i}c_{i}$	steels	[59]
Phase transformation volume fraction	$\chi_{b}=[1-\exp[f_0](-[k(t-t_{1\%})^{n}])]\chi_{max}$ $\chi_{m}=\left[1-\exp\left(-k_{m}(M_{S}-T)\right)\right](1-\chi_{b})$	boron-bearing 0.2 C steel	[12]

Critical stress	$\sigma_{C-\gamma}=\frac{\Delta G_{\gamma-\alpha}+\sigma_{YS-\alpha}}{[1-(0.5)(0.22)-(0.707)(0.03)]}$	C-Mn steel	[60]

AI IN STEEL RESEARCH

AI refers to computational systems capable of learning from and interpreting complex datasets[61]. ML, a core subset of AI, integrates methodologies from computer science, probability theory, and statistics. By harnessing large-scale datasets and sophisticated algorithms, ML empowers computers to replicate aspects of human cognition, continuously enhancing performance and decision-making through iterative improvement. The efficacy of ML models is fundamentally contingent upon the quality, diversity, and volume of training data. In steel manufacturing, the vast datasets accumulated during processing and quality control have catalyzed significant advancements in data-driven materials research. This section outlines the key principles of ML and critically assesses recent breakthroughs in steel research.

Basic principles and functional algorithms of ML

Since the 1950s, AI has evolved from rudimentary machine reasoning to sophisticated ML paradigms. Today, ML excels at extracting intricate patterns from high-dimensional datasets, offering efficient solutions to complex materials problems[2]. The typical ML workflow, analogous to facets of human cognition, is characterized by sequential information processing and iterative refinement of predictive algorithms. The ML process typically comprises three principal stages: data input, model learning and training, and data output, as depicted in Figure 4. The data input stage involves the systematic acquisition and rigorous pre-processing of relevant information. Ensuring data integrity is paramount, as both the structure and quality of the dataset profoundly affect model reliability and predictive accuracy[62]. In materials science, input data are derived from experimentally measurements or computationally simulations, such as chemical composition, processing parameters, and microstructure features. A central goal is to accurately predict the properties of novel materials beyond the training set.

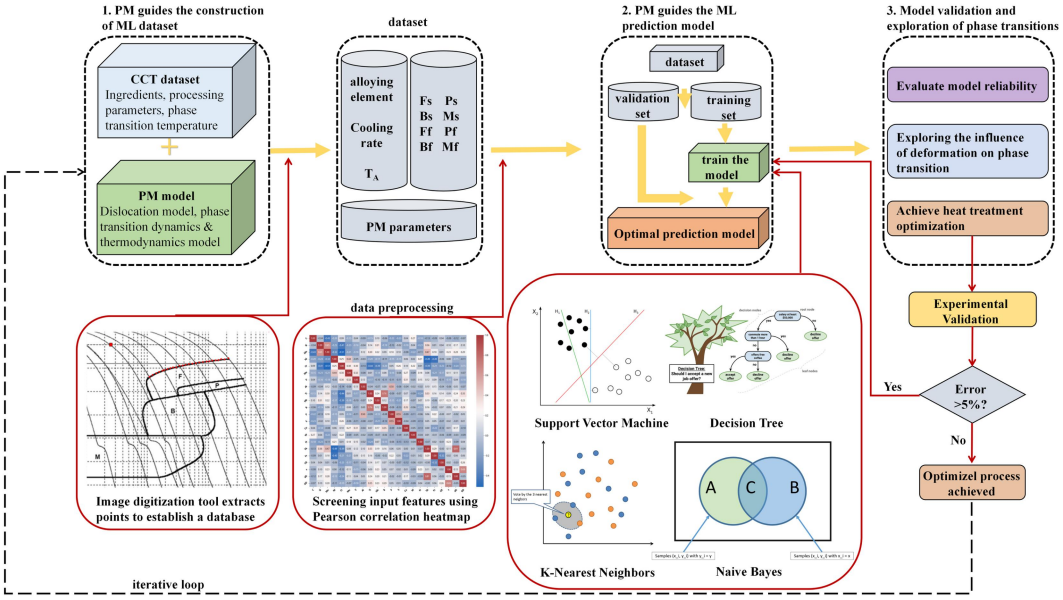

Figure 4. Workflow of PM-guided machine learning for steel phase transformation prediction.

Achieving robust predictive performance requires meticulous attention to data provenance. Datasets often originate from heterogeneous sources, where inconsistencies in standardization and instrumentation can introduce confounding variables. Furthermore, restricted sample sizes may constrain model generalizability and increase susceptibility to overfitting. Addressing these data-centric challenges is imperative for unlocking the full potential of ML-driven advancements in materials science. After assembling the foundational dataset, researchers commonly encounter anomalies, missing values, and inconsistencies. As a result, comprehensive data pre-processing, including outlier identification, imputation of missing data, normalization, and standardization, is an essential prerequisite to ensure data quality and reliability before proceeding to model training and evaluation.

Data preprocessing represents a fundamental and indispensable stage in ML pipeline, encompassing both data cleaning and feature engineering. Data cleaning entails the rigorous identification and correction of incomplete, inconsistent, or erroneous records, thereby safeguarding the reliability and validity of the dataset. Feature engineering

focuses on the systematic selection, transformation, and synthesis of variables that exhibit strong predictive relevance to the target outcome. Common techniques such as correlation analysis, dimensionality reduction, and domain-informed transformations are frequently employed to optimize feature sets. This multifaceted process not only improves model interpretability but also boosts predictive accuracy and generalizability. Furthermore, the creation of novel features through mathematical manipulation or aggregation of existing variables enables more sophisticated and context-sensitive analyses, ultimately advancing the depth and precision of research findings.

During the learning and training stage, ML algorithms discern complex patterns and latent relationships. The development of predictive models follows a structured approach: (1) algorithm selection aligned with data characteristics; (2) performance evaluation using cross-validation and statistical metrics; and (3) hyperparameter optimization. ML methodologies are broadly categorized into supervised, unsupervised, semi-supervised and reinforcement learning paradigms. Supervised learning involves training models on labeled datasets, which facilitates the identification of explicit relationships between input variables and corresponding outcomes. This methodology is fundamental to tasks like classification and regression. In contrast, unsupervised learning utilizes only input data, enabling models to discover inherent patterns, clusters, or latent features without predefined labels. Semi-supervised learning combines elements of both by utilizing datasets that include both labeled and unlabeled examples, thereby enhancing model accuracy and generalizability. Reinforcement learning requires an agent to interact with its environment, make sequential decisions, and adjust its strategy based on feedback in the form of rewards or penalties. Through repeated trial-and-error, the agent optimizes its actions to maximize cumulative rewards, making reinforcement learning particularly suitable for applications in robotics, adaptive control, and complex game strategies[62,63]. The selection of a suitable ML algorithm depends on the specific characteristics and requirements of the research problem. Algorithms differ in their strengths, limitations, and performance profiles according to data type, dimensionality, and task objectives. Table 2 summarizes several widely used ML

algorithms, including Logistic Regression (LR), K-Nearest Neighbor (K-NN), Support Vector Machine (SVM), and Artificial Neural Network (ANN), and classifies them by their functional principles and typical application domains[64,65].

In model development, datasets are typically divided into subsets: a training set for model fitting and a test set for evaluating generalization to new data. The strategy used for this partitioning can have a substantial impact on model accuracy, robustness, and the reliability of performance metrics. While the hold-out method, relying on a single random split, is simple, it can result in unbalanced or unrepresentative samples, introducing bias or instability into performance estimates. To address these limitations, cross-validation methods like k-fold cross-validation are widely adopted[2]. In approach-fold cross-validation, the dataset is split into k mutually exclusive folds. The model is trained on k-1 folds and validated on the remaining fold, with the process repeated k times so that each fold serves as the validation set once. This methodology enables a more robust and comprehensive evaluation of model performance, reduces sensitivity to data partitioning, and provides a more accurate estimate of generalizability.

Finally, selecting appropriate evaluation metrics is essential and should be tailored to the specific task and objectives. For classification tasks, metrics include Accuracy, Precision, Recall, and F1 score, each measuring specific aspects of model discrimination using counts of true positives (TP), true negatives (TN), false positives (FP), and false negatives (FN). For regression key metrics include mean absolute error (MAE), root mean squared error (RMSE), mean squared error (MSE), and the coefficient of determination (R^2), which together assess both the magnitude of prediction errors and the capacity of model to explain variance in the data. Table 3 presents the detailed formulas for each metrics to support transparent and objective model assessment.

Table 2. Common algorithms and main tasks of ML.

Algorithm type	Algorithm	Task	Reference
Supervised Learning	Linear Regression	Regression	[66]
	LR		[67]
	Lasso Regression		[68]
	Support Vector Regression (SVR)		[69]
	ANN		[70]
	Decision tree	Classification	[71]
	K-NN		[72]
	Naive Bayes		[73]
	Support Vector Classification		[74]
Unsupervised Learning	K-Means	Clustering	[75]
	Density-Based Spatial Clustering of Applications with Noise (DBSCAN)		[76]
	Agglomerative Clustering		[77]
	Principal Component Analysis	Dimensionality reduction	[78]
	Linear Discriminant Analysis		[78]

Table 3. Evaluation indicators of Machine Learning

Task	Evaluation indicators	Calculation formula
Classification	Accuracy	$\text{Accuracy} = \frac{TP+TN}{TP+TN+FP+FN}$
	Precision	$\text{Precision} = \frac{TP}{TP+FP}$

	Recall	$\text{Recall} = \frac{\text{TP}}{\text{TP+FN}}$
	F_1 score	$F_1 = \frac{2 \times \text{Precision} \times \text{Recall}}{\text{Precision+Recall}}$
Regression	MAE	$\text{MAE} = \frac{1}{n}\sum_{i=1}^{n}\lvert\hat{y}_i - y_i\rvert$
	RMSE	$\text{RMSE} = \sqrt{\frac{1}{n}\sum_{i=1}^{n}(\hat{y}_i - y_i)^2}$
	MSE	$\text{MSE} = \frac{1}{n}\sum_{i=1}^{n}(\hat{y}_i - y_i)^2$
	R^2	$R^2 = 1 - \frac{\sum_{i=1}^{n}(\hat{y}_i - y_i)^2}{\sum_{i=1}^{n}(\bar{y}_i - y_i)^2}$

ML model in steel design and optimization

Accelerating the discovery of advanced materials while reducing development costs remain key goals in materials science. Alloying offers a vast design landscape for tailoring mechanical properties to fulfill diverse application demands[79]. Traditionally, alloy design focused on one or two principal elements, with additional alloying components incorporated to achieve targeted performance criteria. In steels, Fe serves as the foundational element, while precise control of C, Mn, Si, Cr, and other alloying elements enables the engineering of desired microstructure and properties. The interplay among composition, processing, and microstructure exerts a profound influence on the resulting material properties.

Computational simulation-guided approaches have profoundly transformed materials design, delivering significant advancements beyond conventional trial-and-error methods. First-principles techniques like density functional theory (DFT) offer atomic-scale insights for well-defined materials, but their applicability is limited in the context of complex alloys. Molecular dynamics (MD) and Monte Carlo (MC)

simulations facilitate the modeling of large-scale systems, yet their predictive accuracy diminishes with increasing system complexity and compositional diversity[80]. The Calculation of Phase Diagrams (CALPHAD) framework remains fundamental for thermodynamic predictions, yet struggles with the multidimensional interactions inherent in advanced alloys[53,63]. However, as the materials data becomes more expansive and complex, traditional computational methodologies face increasing limitations in capturing the nuanced and multidimensional interactions inherent in advanced alloy systems. In this context, data-driven ML models have emerged as powerful tools for elucidating the intricate links among composition, processing, and performance. ML enables rapid, on-demand material design and supports inverse engineering of parameters to target specific property profiles, increasingly aligning with the evolving demands of the steel industry[81], see in Figure 4.

Recent advances illustrate the significant impact of ML on alloy design and optimization. Dutta *et al.*[52] combined ANN with multi-objective genetic algorithm (GA) to optimize the strength-ductility balance in dual-phase (DP) steel. Shen *et al.*[82] established a framework integrating PM principles with ML-based regression and classification, successfully developing ultra-high-strength stainless steel. Wei *et al.*[83] employed transfer learning, using a Convolutional Neural Network (CNN) to predict quasi-static properties and link them to fatigue strength, enabling efficient high-throughput design. Liu *et al.*[84] utilized Gaussian process regression (GPR) and genetic algorithm artificial neural networks (GAANN) to model high-manganese steels, balancing performance with cost-effectiveness via the NSGA-II algorithm. Hu *et al.*[85] combined adaptive learning with thermodynamic modeling to construct a Laves phase database, facilitating the successful design of a novel 15Cr ferrite steel. Collectively, these studies highlight the pivotal role of ML in revolutionizing steel development. Data-driven ML methodologies have become indispensable for the rapid, efficient, and targeted design of high-performance steels[81].

Traditional material design methods often struggle to achieve precise property targets,

leading to labor-intensive experiments and repeated cycles of trial and error. Such processes are often characterized by prolonged development timelines, low efficiency, elevated costs, and a dependence on serendipitous discoveries. In continuous production, even minor process variations can compromise batch quality. Consequently, integrating multi-process data to establish seamless links among design, processing, and performance is a critical focus[54].

ML has been extensively applied to predict heat treatment conditions, process parameters and the properties of steels. The prevailing methodology involves constructing databases comprising chemical composition, processing variables, and performance metrics to enable accurate screening and selection of steel properties. This data-centric paradigm supports on-demand material design tailored to specific property requirements. ML prediction models map material parameters (inputs) to targeted material properties (outputs), with continuous improvements in model architectures and feature selection. Notably, many ML models now achieve predictive accuracy comparable to experimental measurements. The following section provides a concise overview of recent research advances in ML-based prediction of steel properties.

Guo *et al.*[86] utilized ANN to capture the complex relationships among alloy composition, process parameters, and both physical and mechanical properties of maraging steel. Li *et al.*[10] pioneered an integrated thermo-mechanical-metallurgical framework that incorporates a deep-learning-based phase transformation (DLPT) model to predict the mechanical behavior of hot-stamped parts. Geng *et al.*[87] utilized material descriptors, including chemical composition and Jominy bar distance, to build a data-driven ML model that accurately predicts the hardenability curves for boron steels, providing valuable guidance for alloy design and heat-treatment optimization. Millner *et al.*[55] established multiple ML models to forecast key mechanical properties, i.e., plastic strain ratio, tensile strength, yield stress, and elongation at fracture, for steel coils, systematically evaluating the influence of hyperparameter tuning on predictive accuracy. Collectively, these studies demonstrate the exceptional potential of ML models in

forecasting steel properties. Researchers have further enhanced model interpretability by applying Shapley additive explanations (SHAP) to elucidate the influence of input features and analyze the complex interactions between alloying elements and target properties[56-58,88,89].

Building on the robust predictive power of ML models, bidirectional design strategies have been developed to link chemical composition and properties. Li *et al.*[59] introduced a model linking composition, heat treatment, and tensile properties for reduced-activation ferritic/martensitic (RAFM) steel. This approach enabled the development of a novel alloy with superior performance. Trzaska *et al.*[60] employed ANN and GA to elucidate the relationships among chemical composition, austenitizing temperature, and post-cooling hardness, thereby enabling the calculation of steel compositions optimized for quenching and tempering to achieve targeted hardness levels.

ML MODELLING PREDICTS CONTINUOUS COOLING TRANSFORMATION

The urgent need for efficient generation of TTT and CCT diagrams has driven the adoption of computational strategies[46]. Employing computer technology to tackle this critical challenge has emerged as a highly promising strategy in data-driven era. Early on, computational methods enabled two main strategies: (1) using databases to quickly retrieve CCT diagrams for steels with similar chemical compositions and austenitizing temperatures, and (2) employing mathematical models, empirical formulas, and more recently, AI methods to derive phase transformation temperatures and curves[7,90]. Recent advancements position data-driven ML as a vital tool for rapid materials discovery. Unlike physics-based approaches, ML adeptly circumvent complex mathematical formulations and physical mechanism assumptions, establishing robust multivariate nonlinear relationships between inputs and outputs directly from data. This unique capability renders ML exceptionally well-suited for multidimensional challenges in materials science, enabling swift extraction of key insights from large datasets and

delivering accurate predictions for new alloys. Consequently, the application of ML in predicting CCT diagrams for steels has attracted significant attention[90-93], with numerous researchers utilizing neural networks and other ML algorithms to advance the filed[54,94,95].

Considerable research has focused on synthetic HAZ continuous cooling transformation (SH-CCT) diagrams[96]. Geng *et al.*[97] employed random forest (RF) algorithm to predict the starting temperatures of ferritic and bainitic transformation, and the K-NN algorithm for martensite start temperatures and the Random Committee (RC) method to predict hardness across varying cooling rates. The established ML model not only successfully predicted the SH-CCT diagram, achieving correlation coefficients exceeding 0.8, but also demonstrated the potential of ML in this field though their models were tailored specifically to Ni-Cr-Mo steel. Minamoto *et al.*[94] enhanced prediction robustness using RF method with double cross-validation (DCV), carefully accounting for critical factors such as cooling rates and transformation start temperatures. Geng *et al.*[95] adopted a hybrid approach, integrating multilayer perceptron classifiers (MPC), K-NN, and RF to derive symbolic regression expressions for hardness. Zhang *et al.*[98] proposed an optimized ML model that combining back propagation (BP) and radial basis function (RBF) neural network, showcasing exemplary generalization capabilities on external datasets when predicting SH-CCT diagrams for various steels, see in Figure 5.

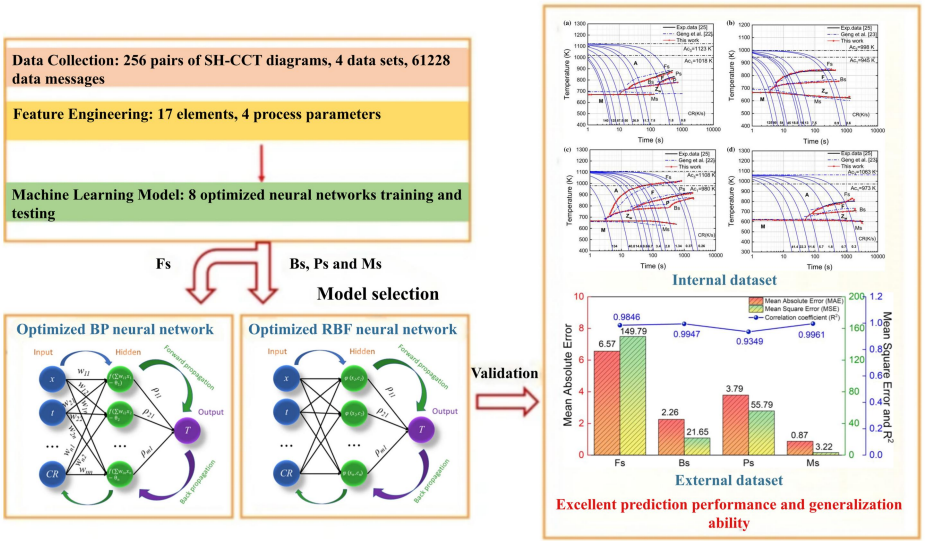

Figure 5. Machine learning pipeline for predicting CCT curve via optimized BP and RBF neural networks. Copyright 2023, Springer Nature, Reproduced with permission[98].

Beyond CCT curves, ML models targeting specific phase transformation temperatures have achieved high accuracy and provided detailed analyses of feature importance and underlying mechanisms. Rahaman *et al.*[99] applied four different ML ensemble algorithms, including RF, Extremely Randomized Trees (ERT), Gradient Boosting (GB), and AdaBoost (AB), to predict the martensite start temperature(M_s). Their findings compellingly demonstrate that this approach not only surpasses Traditional ANN on smaller datasets but also showcases exceptional performance on validation datasets. Similarly, Jeon *et al.* utilized RF regression to predict the bainite start temperature(B_s)[56], used an ANN for M_s predictions[58], employing SHAP analysis to interpret feature importance and models behavior. Moreover, Zhang *et al.*[57] used an enhanced gradient boosting model (LightGBM) to investigate the influence of alloying elements on critical temperatures (Ac_1, Ac_3, M_s, B_s), utilizing partial dependence plots (PDP) and SHAP methods to elucidate mechanisms.

As early as 2004, Trzaska and Dobrzański[90] pioneered the use of neural networks to forecast the CCT diagram of steel, modeling chemical composition, austenitizing

temperature, and empirical CCT data to systematically evaluate the influence of these factors on low-alloyed structural steels. By 2007, their research had evolved to incorporate ANNs and regression methods, elucidating intricate relationships among chemical composition, critical and transformation temperatures, and transformation times via multiple regression (MR) analyses. ANNs further facilitated the predictions of individual phase transformations over a full range of cooling rates[7]. Trzaska subsequently refined ANN architectures and developed novel techniques for constructing CCT diagram[92], thereby establishing a robust foundation for ML integration in CCT diagram prediction. In 2017, Chakraborty *et al.*[91] further advanced ANN architectures utilizing error backpropagation multilayer perceptron (MLP), incorporating multi-objective optimization strategies to mitigate prediction error. The subsequent integration of multi-criteria decision-making (MCDM) techniques by Chakraborty *et al.*[93] in 2018 restructured the optimization framework into a single-objective paradigm, streamlining computational requirements, though with a modest reduction in model fidelity. More recently, Geng *et al.*[8] explored a suite of ML algorithms, including MLP, K-NN, bagging, and RF, for predict CCT diagrams in tool steels, comparing algorithm performance for various transformation temperatures and ultimately selecting the optimal model. The validity of this model was corroborated through comparison with both experimental and CCT diagrams generated by JMatPro.

Overall, these ML strategies have significantly enhanced the efficiency and accuracy of CCT diagram development, see in Table 4. Furthermore, they facilitate the integration of materials informatics and MGE into steel research, accelerate process optimization and alloy design, and fully harness the potential of big data analytics within materials science.

Table 4. Summary of ML models for phase transformation temperature predictions in literature.

Predicted Target	ML algorithm	Database input	Database source	Alloy	Reference
F_s, B_s, M_s, Hardness	K-NN, RC, RF, MLP	Compositions, Cooling rate	NIMS Materials Database	Ni-Cr-Mo steel	[97]
Ac_3, F_s, P_s, B_s, M_s	RF, MR, SVR XGBoost	Compositions	NRIM Atlas 1	Structural steel	[94]
F_s, P_s, B_s, M_s, P_f, Hardness	MLP, SVR, RF RBF, K-NN	Compositions, Cooling rate	Japan National Institute of Material Science database	Low alloy steel	[95]
F_s, P_s, B_s, M_s	The BP and RBF neural networks	Compositions, Transformation time, Ac_1, Cooling rate	NIMS Materials Database	Steels	[98]
M_s	RF, ERT, GB, AB	Compositions	Literature	Steels	[99]
B_s	RFR, ANN, K-NN	Compositions, Austenite average grain size	Literature	Low alloy steel	[62]
M_s	RFR, SVR, K-NN	Compositions, Austenite average grain size	Literature	Alloy steel	[64]

M_s, B_s, Ac_1, Ac_3	LightGBM	Compositions, Heating Rate, Cooling rate, Atomic parameters	Materials Algorithms Project	Steels	[51]
F_s, F_f, P_s, P_f, B_s, B_f	MLP, GRNN	Compositions, Cooling rate, T_A	Literature	Constructional steel, machinable steel	[90]
Ac_1, Ac_3, F_s, P_s, B_s, M_s, t_F, t_B, t_P	MLP	Compositions, Cooling rate, T_A	Literature	Engineering steel, Constructional steels	[7]
Ac_1, Ac_3, F_s, P_s, B_s, M_s, F_f, P_f, B_f, Hardness,	ANN	Compositions, Cooling rate, T_A	Literature	Structural steel, Engineering steel	[92]
F_s, P_s, B_s, F_f, P_f, B_f,	ANN	Compositions, Cooling rate, T_A	Literature	Low carbon steel	[91,93]
P_s, P_f, B_s, B_f, M_s	MLP, K-NN, Bagging, RF	Compositions, Cooling rate, T_A	Literature	Tool steel	[8]

RFR: Random Forest Regressor; GRNN: Generalized Regression Neural Network; Bagging: Bootstrap Aggregating.

Physical metallurgy-guided ML methods

While ML has revolutionized the prediction of CCT diagrams, a significant gap remains in incorporating processing conditions and their direct effects on phase transformations in contemporary predictive models. The successful design and production of advanced steels increasingly rely on the precise tailoring of microstructure-property relationships, often achieved through thermo-mechanically controlled processes (TMCPs) such as hot deformation. State-of-the-art simulations, elucidate critical physical metallurgical phenomena, namely, dynamic/static recrystallization, grain growth, and phase transformations, that occur during steel deformation[100-105]. These experiments yield invaluable mechanistic insights into phase transformations governed by thermodynamic and kinetic factors under non-equilibrium processing conditions, see in Figure 6A.

To advance the field, next generation of ML-driven predictive frameworks must systematically integrate these experimentally derived physical metallurgical phenomena, thereby enhancing accuracy and generalizability across a broader range of steel manufacturing scenarios. This section provides a comprehensive review of advanced physical metallurgical models describing steel deformation behavior, discusses methodological strategies for fusing these models with ML algorithms, and outlines practices for selecting relevant supplementary input features. Key considerations for developing rigorous, physically grounded ML models are also explored.

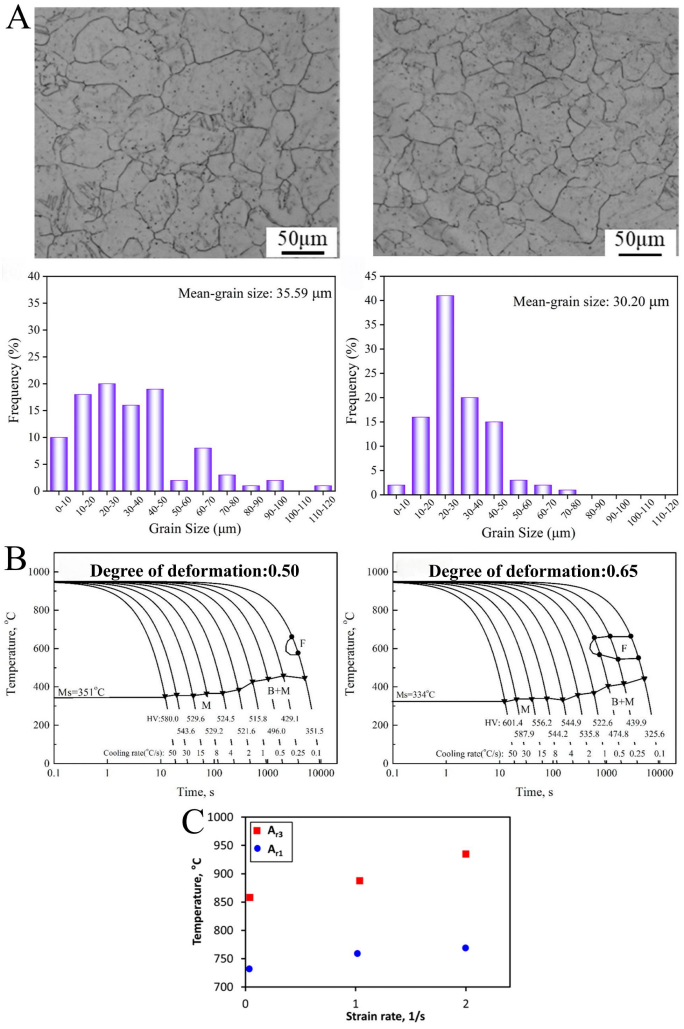

Figure 6. (A) Microstructural changes in steel processed under recrystallization conditions (1,150-1,100 °C) and non-recrystallization conditions (950-900 °C). Copyright 2021, Wiley-VCH GmbH, Reproduced with permission[106]; (B) Comparison of dynamic CCT curves and phase transformation characteristics for 0.35 and 0.65 strain-deformed steel. Copyright 2019, Wiley-VCH GmbH, Reproduced with permission[31]; (C) Effect of strain rate on the ferritic transformation of HSLA steel. Copyright 2020, MDPI, Reproduced with permission[107].

The deformation behavior of steels arises from a complex interplay of strain, strain rate, and deformation temperature. Capturing the intricate relationships among stress, strain, strain rate, and temperature during deformation remains a significant challenge[108], see in Figure 6. Over the past several decades, constitutive models such as the Arrhenius

equation and the JMAK model have been extensively employed to elucidate how alloying elements and deformation parameters influence material response. A range of theoretical framework has been proposed to elucidate the deformation behavior of steel, encompassing models for flow stress, dislocation dynamics, recrystallization, and phase transformation. Among these, the Arrhenius-type constitutive model, integrating the Zener-Hollomon parameter, has become a foundational tool for characterizing flow stress, as it effectively captures the coupled influence of temperature and strain rate[109]. The corresponding mathematical formulations are presented in Eqs (4)-(6)[13,110-112]:

$$\dot{\varepsilon} = Af(\sigma)\exp\left(-\frac{Q}{RT}\right) \tag{4}$$

$$f(\sigma)=\begin{cases} &\sigma^n \quad \&\&\alpha\sigma<0.8 \\ &\exp(\beta\sigma) \quad \&\&\alpha\sigma>1.2 \\ &[\sinh(\alpha\sigma)]^n \quad \&\&\text{for all } \sigma \end{cases} \tag{5}$$

$$Z = \dot{\varepsilon}\exp\left(\frac{Q}{RT}\right) = A\left[\sinh(\alpha\sigma)\right]^n \tag{6}$$

Where $\dot{\varepsilon}$ denotes the strain rate, A, α, β, n are material-specific constants, Q is the activation energy for deformation, and T is the deformation temperature. The function $f(\sigma)$ characterizes the flow stress σ, while Z is the Zener-Hollomon parameter, which integrates the effects of temperature and strain rate. Furthermore, the austenite-ferrite transformation kinetics model is constructed on the basis of dislocation density and deformation-induced storage energy, facilitating quantitative relationships among dislocation density, stored energy, and flow stress, as described in Eqs. (7) and (8)[14,113]:

$$\sigma = M\alpha Gb\rho^{\frac{1}{2}} \tag{7}$$

$$\Delta G_d = G\rho b^2 \tag{8}$$

Where ρ is the dislocation density, ΔG_d is the dislocation energy, G represents the shear modulus, M is the Taylor factor, b is Burgers vector and α is an empirical constant. Integrating Eqs. (7) and (8) yields Eq. (9), which provides a quantitative relationship between dislocation energy and flow stress, offering deeper insight into the microstructural mechanics underlying deformation:

$$\Delta G_d = \frac{\sigma^2}{M^2 \alpha^2 G} \tag{9}$$

The influence of deformation on phase transformation kinetics has also been extensively examined from the perspective of recrystallization. For instance, Cho *et al.*[15] simulated the static recrystallization behavior of Nb microalloyed steels during hot rolling, deriving the kinetics of static recrystallization using the Avrami equation, as shown in Eq. (10) :

$$X_{SRX} = 1 - \exp\left[-0.693\left(\frac{t}{t_{50\%}}\right)^n\right] \tag{10}$$

Where X_{SRX} is the volume fraction of static recrystallization, t is the elapsed time, $t_{50\%}$ corresponds to the time at which 50% of the volume is recrystallized, and n is the Avrami exponent. Chen *et al.*[16] extended this work by developing a dynamic recrystallization model to quantify the dynamic recrystallization volume fraction, using the Zener-Hollomon parameter as a means to characterize grain size after complete dynamic recrystallization. The mathematical formulation is given in Eq. (11):

$$X_{DRX} = 1 - \exp\left[-0.693\left(\frac{\varepsilon - \varepsilon_c}{\varepsilon_{0.5} - \varepsilon_c}\right)^{n_d}\right] \quad (11)$$

Where X_{DRX} is the volume fraction of dynamic recrystallization, ε_c marks the critical strain for the initiation of dynamic recrystallization, $\varepsilon_{0.5}$ is the strain at 50% dynamic recrystallization and n_d is a material constant determined by linear regression. From a phase transformation perspective, recent studies have introduced sophisticated models to describe transformation kinetics. For example, Li *et al.*[114] performed a systematic investigation of the effects of hot deformation, deformation temperature, and strain rate on phase transformation by integrating *in-situ* isothermal tensile testing, dilatometry, and ex-situ microstructural analysis. Their novel non-isothermal kinetic model incorporates austenite deformation during continuous cooling, enabling precise prediction of final phase fractions and hardness in dynamic CCT scenarios. Similarly, Pohjonen *et al.*[12] developed a kinetic model for austenite-to-bainite and martensite transformations based on the JMAK equation, allowing calibration against experimental data and detailed analysis of the effects of thermomechanical processing conditions on transformation dynamics.

These PM models have been essential for elucidating the relationships among composition, processing, microstructure, and phase transformation mechanisms in steels. However, integrating PM models into ML frameworks while accurately capturing the underlying physical mechanisms remains a significant challenge. Recent advances have addressed this issue by introducing methodologies that incorporate PM-derived information into the ML process by calculating intermediate parameters that serve as supplementary input features[116-119]. This approach has demonstrated an improved ability to represent targeted physical metallurgical phenomena within ML predictions, thereby enhancing model accuracy, see in Figure 7. Li *et al.*[115] used experimental data to establish Arrhenius and dynamic recrystallization models, predicting the influence of

Cu content on the hot deformation behavior of antimicrobial stainless steel. The resulting intermediate parameters were incorporated as additional input features in a least squares support vector machine (LSSVM) model guided by PM, enabling precise prediction of both flow stress and dynamic recrystallization fraction, Similarly, Cui *et al.*[116] applied PM principles to transform high-dimensional rolling process parameters into low-dimensional microstructure features, thereby reducing model overfitting, and then trained a deep neural network (DNN) to predict the yield stress of Ti micro-alloyed steels. Their findings show that DNN predictions informed by PM are more consistent with established metallurgical principles. Li *et al.*[117] further advanced this approach by introducing Ac_1 temperature, Ac_3 temperature, and flow stress as PM-derived features to guide the ML process, developing a generalized model for steel performance prediction.

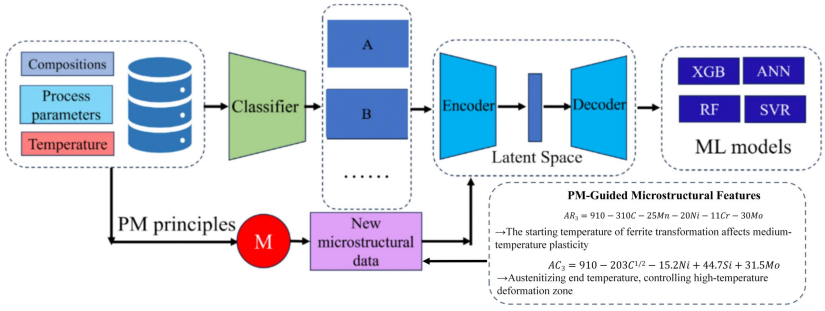

Figure 7. Workflow of the PM-LSF model: PM principles guiding ML for microstructure-related data processing and modeling. Copyright 2025, Springer Nature, Reproduced with permission[118].

This approach maximizes the informational content of the data, enhances data quality, and supports the development of models with strong generalization capabilities grounded in PM. By deriving suitable PM-based supplementary input parameters, such as austenite grain size, deformation storage energy, and diffusion coefficients, researchers can effectively integrate deformation mechanisms into ML-based CCT diagram predictions, offering more robust guidance for industrial design and materials development.

A key challenge is determining which PM parameters best capture the influence of deformation on phase transformation kinetics. Addressing this requires understanding how deformation affects continuous-cooling phase transformations in steels. Extensive research using thermal simulators and dilatometers has investigated the effects of thermal deformation on phase transformation mechanisms during continuous cooling across various steel grades. The consensus is that thermal deformation induces austenite recrystallization and grain refinement. Reduced austenite grain size, elongated grain boundaries, and increased dislocation density and more deformation bands collectively increase nucleation site density and interfacial energy[119-121], thereby accelerating the nucleation kinetics of ferrite, pearlite, and bainite.

Austenite deformation increases stored deformation energy and enhances the efficiency of elemental diffusion, thereby promoting both diffusional (ferrite, pearlite) and semi-diffusional (bainite) phase transformations. Empirical evidence shows that the start curves for ferrite and pearlite transformations shift to lower temperatures in the CCT diagram under deformation, raising their critical cooling rates[122-132]. Bainite transformation proceeds via a shear transformation mechanism, together with carbon diffusion and carbide formation, but its response to deformation and transformation conditions can be complex and sometimes contradictory in the literature[133]. Most studies agree that austenite deformation accelerates the bainite transformation rate, increases the initial transformation temperature, and expands the bainite region in the CCT diagram[134-136]. In contrast, deformation generally has little effect on the non-diffusional martensite transformation, though some reports suggest a marginal decrease in martensite start temperature, particularly with certain alloying elements[124].

These findings demonstrate that grain refinement, increased stored deformation energy, and enhanced diffusion efficiency from austenite deformation significantly influence continuous cooling phase transformations in steel. Thus, selecting PM models associated with austenite grain size, deformation storage energy, and elemental diffusion, and computing the relevant intermediate parameters as supplementary ML inputs, is a

robust strategy for predicting deformation-affected CCT diagrams. see in Figure 7. Cao *et al.*[9] exemplified this approach by developing a CCT prediction model that incorporated calculated austenite grain size and deformation storage energy as input features, using a SVM algorithm and hereditary modeling to optimize post-rolling cooling process design. While the results were promising for HSLA plate steels, further refinement through expanded databases and algorithm comparisons is needed to broaden applicability.

SUMMARY AND OUTLOOK

Recent advances in modeling CCT curves in steels have been driven by the integration of PM and ML methods. While PM provides mechanistic transparency and fundamental insight, ML enables rapid, data-driven predictions and high-throughput screening. However, current models still face major challenges regarding predictive accuracy, computational scalability, and generalizability to next-generation advanced steels, particularly under complex industrial conditions such as hot-rolling and multi-stage processing. Key bottlenecks include:

1) Complexity of Phase Transformation Mechanisms: The influence of trace alloying and rare earth elements on phase transformation kinetics remains poorly understood, and prevailing PMs often rely on oversimplified assumptions, which constrains their capacity to accurately represent the intricate, multivariate interactions characteristic of advanced steel systems.

2) Heterogeneity and Limitations of Data Sources: Experimental and industrial datasets vary widely in quality and standardization. The integration of deformation-related parameters, such as deformation rate, pass schedule, and interpass temperature/time, into comprehensive and unified modeling frameworks continues to present significant technical obstacles.

3) Challenges in Multiphysics Coupling: The coupled effects of thermal, mechanical, and phase transformation phenomena in industrial production environments are inadequately represented within existing unified modeling paradigms. This deficiency compromises the extrapolative robustness and predictive reliability of current models under complex, non-standard processing conditions.

To address these critical bottlenecks, future research must prioritize the following strategic directions:

1) Advancing Mechanistic Understanding of Phase Transformations and Elemental Interactions

Leverage *in-situ* experimental techniques (e.g., synchrotron X-ray diffraction), and multiscale modeling (first-principles calculations and phase-field modeling) to elucidate to elucidate elemental interactions. Embed physical principles into ML architectures via Physics-Informed Neural Networks (PINNs).

2) Optimization and Standardization of Materials Data Infrastructure

Establish robust, multi-source collaborative databases by integrating high-fidelity laboratory datasets with large-scale industrial data. Standardize data architectures to encompass a comprehensive range of steel grades and processing histories, placing particular emphasis on detailed deformation records. Foster cross-sector collaboration to institute unified protocols for data acquisition, annotation, and exchange, thereby enhancing the reusability, reproducibility, and interoperability of CCT-related datasets.

3) Development of Integrated Process-Microstructure-Property Predictive Frameworks

Integrate processing parameters to construct holistic models capable of resolving the complex interactions among deformation, thermal history, and phase evolution, thereby

enabling end-to-end prediction of process-microstructure relationships. Link CCT-based microstructural outputs to downstream performance models, such as crystal plasticity finite element simulations or ML-based surrogates, to facilitate simultaneous, high-fidelity prediction of key mechanical properties and performance metrics.

DECLARATIONS

Authors' contributions

Data curation (lead); formal analysis (lead); investigation (lead); methodology (lead); visualization (lead); writing - original draft (lead); writing - review and editing (lead): H.R, Z.W;

Data curation; formal analysis; investigation: Y.J, W.Y, Y.H;

Conceptualization (lead); supervision (lead); visualization; writing - review and editing (lead): H.X, Hou.Z.

Availability of data and materials

The data and source code that support the findings of this study are available from the corresponding authors upon reasonable request.

AI and AI-assisted tools statement

Not applicable.

Financial support and sponsorship

The authors would like to thank the financial support by National Key Research and Development Program of China (2024YFB3713703), National Natural Science Foundation of China (52574428), the Foundation for Innovative Research Groups of the National Natural Science Foundation of China (T2421001), the Fundamental Research Funds for the Central Universities (2024IAIS-ZD004) and State Key Laboratory of Mechanical Transmission for Advanced Equipment under the grant (SKLMT-ZZKT-2024Z04).

Conflicts of interest

All authors declared that there are no conflicts of interest.

Copyright

REFERENCES

1. Geng, X. X.; Wang, F. Y.; Wu, H. H.; et al. Data-driven and artificial intelligence accelerated steel material research and intelligent manufacturing technology. *Materials Genome Engineering Advances* **2023,** *1(1)*, 86-103.[DOI: 10.1002/mgea.10]

2. Fang, W.; Huang, J. X.; Peng, T. X.; Long, Y.; Yin, F. X. Machine learning-based performance predictions for steels considering manufacturing process parameters: A review. *Journal of Iron and Steel Research International* **2024,** *31*, 1555-81.[DOI: 10.1007/s42243-024-01179-5]

3. Yu, X.; Tan, C. China?S pathway to carbon neutrality for the iron and steel industry. *Global Environmental Change-Human and Policy Dimensions* **2022,** *76*, 102574.[DOI: 10.1016/j.gloenvcha.2022.102574]

4. Li, Y. B.; Li, J.; Sun, M.; et al., Analysis of carbon neutrality technology path selection in the steel industry under policy incentives. *Energy* **2024,** *292*, 130550.[DOI: 10.1016/j.energy.2024.130550]

5. Kang, Z.; Liao, Q.; Zhang, Z.; Zhang, Y. Carbon neutrality orientates the reform of the steel industry. *Nat Mater* **2022,** *21*, 1094-8.[DOI: 10.1038/s41563-022-01370-7]

6. Gutiérrez Castañeda, E. J.; Ruiz Cigarrillo, D.; Torres Castillo, A.; et al. Intercritical continuous cooling transformation diagram for the manufacture of low-alloyed low-carbon multiphase steels. *Materials Letters* **2023,** *331*, 133528.[DOI: 10.1016/j.matlet.2022.133528]

7. Trzaska, J.; Dobrzanski, L. A. Modelling of cct diagrams for engineering and constructional steels. *Journal of Materials Processing Technology* **2007,** *192*, 504-10.[DOI: 10.1016/j.jmatprotec.2007.04.099]

8. Geng, X. X.; Wang, H.; Xue, W. H.; et al. Modeling of cct diagrams for tool steels

using different machine learning techniques. *Computational Materials Science* **2020,** *171*, 109235.[DOI: 10.1016/j.commatsci.2019.109235]

9. Cao, Y.; Cao, G. M.; Cui, C. Y.; et al., Modeling continuous cooling transformations for hsla steels with physical metallurgy guided hereditary machine learning. *Metallurgical and Materials Transactions a-Physical Metallurgy and Materials Science* **2023,** *54*, 4891-904.[DOI: 10.1007/s11661-023-07210-w]

10. Li, Y. F.; Li, S. H. Deep learning based phase transformation model for the prediction of microstructure and mechanical properties of hot-stamped parts. *International Journal of Mechanical Sciences* **2022,** *220*, 107134.[DOI: 10.1016/j.ijmecsci.2022.107134]

11. Pei, Y.; Gao, Z.; Liu, Y.; et al. Continuous cooling transformation behavior and the phase transformation model in low carbon high strength sheet steel. In *PROCEEDINGS OF 2014 INTERNATIONAL CONFERENCE ON MATERIAL SCIENCE AND ENGINEERING*, 2014-01-01; 2014; Vol. 1035, pp 27-+.[DOI: 10.4028/www.scientific.net/AMR.1035.27]

12. Pohjonen, A.; Somani, M.; Porter, D. Modelling of austenite transformation along arbitrary cooling paths. *Computational Materials Science* **2018,** *150*, 244-51.[DOI: 10.1016/j.commatsci.2018.03.052]

13. Hatta, N.; Kokado, J.; Kikuchi, S.; Takuda, H. Modeling on flow-stress of plain carbon-steel at elevated-temperatures. *Steel Research* **1985,** *56*, 575-52.[DOI: 10.1002/srin.198500694]

14. Suwanpinij, P.; Rudnizki, J.; Prahl, U.; Bleck, W. Investigation of the effect of deformation on γ-α phase transformation kinetics in hot-rolled dual phase steel by phase field approach. *Steel Research International* **2009,** *80*, 616-22.[DOI: 10.2374/Sri09sp047]

15. Cho, S.-H.; Kang, K.-B.; Jonas, J. J. Mathematical modeling of the recrystallization kineticsof nb microalloyed steels. *ISIJ international* **2001,** *41*, 766-73.[DOI: 10.2355/isijinternational.41.766]

16. Chen, X. M.; Lin, Y. C.; Wen, D. X.; Zhang, J. L.; He, M. Dynamic recrystallization behavior of a typical nickel-based superalloy during hot deformation. *Materials &*

Design **2014,** *57*, 568-77.[DOI: 10.1016/j.matdes.2013.12.072]

17. Wang, W. Y.; Zhang, S. Y.; Li, G. N.; et al. Artificial intelligence enabled smart design and manufacturing of advanced materials: The endless frontier in ai era. *Materials Genome Engineering Advances* **2024,** *2*, e56.[DOI: 10.1002/mgea.56]

18. Xu, P. C.; Ji, X. B.; Li, M. J.; Lu, W. C. Small data machine learning in materials science. *Npj Computational Materials* **2023,** *9*, 42.[DOI: 10.1038/s41524-023-01000-z]

19. Ghazali, S. N. M.; Ibrahim, M. H. I.; Manurung, Y. H. P.; et al. A focused review on numerical computation in wire arc additive manufacturing for high strength low alloy steels: Past insights and potential opportunities. *International Journal of Advanced Manufacturing Technology* **2025,** *141*, 2679-708.[DOI: 10.1007/s00170-025-16817-9]

20. Avrami, M. Kinetics of phase change i - general theory. *Journal of Chemical Physics* **1939,** *7*, 1103-12.[DOI: 10.1063/1.1750380]

21. Avrami, M. Kinetics of phase change. Ii transformation-time relations for random distribution of nuclei. *The Journal of chemical physics* **1940,** *8*, 212-24.[DOI: 10.1063/1.1750631]

22. He, J. J.; Su, X. P.; Wang, C. X.; et al. Machine learning assisted predictions of multi-component phase diagrams and fine boundary information. *Acta Mater* **2022,** *240*, 118341.[DOI: 10.1016/j.actamat.2022.118341]

23. Qiao, L.; Zhu, J. C.; Wang, Y. Machine learning-aided process design: Modeling and prediction of transformation temperature for pearlitic steel. *Steel Research International* **2022,** *93*, 2100267.[DOI: 10.1002/srin.202100267]

24. Leblond, J.-B.; Devaux, J.; Devaux, J. Mathematical modelling of transformation plasticity in steels i: Case of ideal-plastic phases. *International journal of plasticity* **1989,** *5*, 551-72.[DOI: 10.1016/0749-6419(89)90001-6]

25. Hedström, P.; Cubero, V. L.; Sigurdsson, J.; et al. Physics-informed machine learning for steel development: A computational framework and cct diagram modeling. *Metallurgical and Materials Transactions A* **2026**.[DOI: 10.1007/s11661-026-08181-4]

26. Kirkaldy, J. S. Prediction of alloy hardenability from thermodynamic and kinetic data. *Metallurgical Transactions* **1973,** *4*, 2327-33.[DOI: 10.1007/Bf02669371]

27. Olson, G.; Cohen, M. Reply to “on the equilibrium temperature in thermoelastic

martensitic transformations". *Scripta Metallurgica* **1977,** *11*, 345-7.[DOI: 10.1016/0036-9748(77)90264-2]

28. Andersson, J. O.; Helander, T.; Höglund, L. H.; Shi, P. F.; Sundman, B. Thermo-calc & dictra, computational tools for materials science. *Calphad-Computer Coupling of Phase Diagrams and Thermochemistry* **2002,** *26*, 273-312.[DOI: 10.1016/S0364-5916(02)00037-8]

29. Zhang, S.; Zhang, C.; Han, X.; Wang, B. Mrf-pinn: A multi-receptive-field convolutional physics-informed neural network for solving partial differential equations. *Computational Mechanics* **2024,** *75*, 1137-63.[DOI: 10.1007/s00466-024-02554-5]

30. Leng, J. W.; Zuo, K. W.; Xu, C. Y.; et al. Physics-informed machine learning in intelligent manufacturing: A review. *Journal of Intelligent Manufacturing* **2025**, 1-43.[DOI: 10.1007/s10845-025-02641-1]

31. Li, J.; Tan, Z. L.; Zhang, M.; et al., On the significant impact of deformation coupled with cooling rate during thermo-mechanical controlled processing (tmcp) on microstructure-property relationship in 25mn2si2cr high strength steel. *Steel Research International* **2019,** *90*, 1900134.[DOI: 10.1002/srin.201900134]

32. Liu, H. A.; Xu, D.; Pang, H. X.; Yin, X.; Wang, X. Y.; Zheng, B. Analysis of isothermal transformation behavior and phase transformation kinetic model for 20mntib steel. *Transactions of the Indian Institute of Metals* **2025,** *79(1)*, 7.[DOI: 10.1007/s12666-025-03761-1]

33. Zhao, H.; Hu, X. L.; Cui, J. J.; Xing, Z. W. Kinetic model for the phase transformation of high-strength steel under arbitrary cooling conditions. *Metals and Materials International* **2019,** *25*, 381-95.[DOI: 10.1007/s12540-018-0196-2]

34. Fanfoni, M.; Tomellini, M. The johnson-mehl-avrami-kohnogorov model: A brief review. *Il Nuovo Cimento D* **1998,** *20*, 1171-82.[DOI: 10.1007/BF03185527]

35. Chen, X. J.; Xiao, N. M.; Li, D. Z.; Li, G. Y.; Sun, G. Y. The finite element analysis of austenite decomposition during continuous cooling in 22mnb5 steel. *Modelling and Simulation in Materials Science and Engineering* **2014,** *22*, 065005.[DOI: 10.1088/0965-0393/22/6/065005]

36. Cahn, J. W. Transformation kinetics during continuous cooling. *Acta Metallurgica*

1956, *4*, 572-5.[DOI: 10.1016/0001-6160(56)90158-4]

37. Liu, F.; Yang, C.; Yang, G.; Zhou, Y. Additivity rule, isothermal and non-isothermal transformations on the basis of an analytical transformation model. *Acta Mater* **2007,** *55*, 5255-67.[DOI: 10.1016/j.actamat.2007.05.041]

38. Scheil, E. Anlaufzeit der austenitumwandlung. *Archiv für das Eisenhüttenwesen* **1935,** *8*, 565-7.[DOI: 10.1002/srin.193500186]

39. Kirkaldy, J. Prediction of microstructure and hardenability in low alloy steels. *In Proceedings of the International Conference on Phase Transformation in Ferrous Alloys, 1983*, AIME: 1983.

40. Koistinen, D. P.; Marburger, R. E. A general equation prescribing the extent of the austenite-martensite transformation in pure iron-carbon alloys and plain carbon steels. *Acta Metallurgica* **1959,** *7*, 59-60.[DOI: 10.1016/0001-6160(59)90170-1]

41. Collins, J.; Piemonte, M.; Taylor, M.; Fellowes, J.; Pickering, E. A rapid, open-source cct predictor for low-alloy steels, and its application to compositionally heterogeneous material. *Metals* **2023,** *13*, 1168.[DOI: 10.3390/met13071168]

42. Umemoto, M.; Hiramatsu, A.; Moriya, A.; et al. Computer modeling of phase-transformation from work-hardened austenite. *Isij International* **1992,** *32*, 306-15.[DOI: 10.2355/isijinternational.32.306]

43. Lee, K. J.; Lee, J. K. Modelling of γ/α transformation in niobium-containing microalloyed steels. *Scripta Materialia* **1999,** *40*, 831-6.[DOI: 10.1016/S1359-6462(99)00025-1]

44. Li, M. V.; Niebuhr, D. V.; Meekisho, L. L.; Atteridge, D. G. A computational model for the prediction of steel hardenability. *Metallurgical and Materials Transactions B-Process Metallurgy and Materials Processing Science* **1998,** *29*, 661-72.[DOI: 10.1007/s11663-998-0101-3]

45. Zhang, M.; Zhang, B. D.; Tian, Y. B.; et al. Continuous heating/cooling transformation kinetics of a novel crnimov steel for large structural parts. *Steel Research International* **2023,** *94(12)*.[DOI: 10.1002/srin.202300226]

46. Saunders, N.; Guo, Z.; Li, X.; Miodownik, A.; Schillé, J. P. The calculation of ttt and cct diagrams for general steels. *JMatPro Software Literature* **2004,** *2*.

47. Martin, H.; Amoako-Yirenkyi, P.; Pohjonen, A.; Frempong, N. K.; Komi, J.; Somani, M. Statistical modeling for prediction of cct diagrams of steels involving interaction of alloying elements. *Metallurgical and Materials Transactions B-Process Metallurgy and Materials Processing Science* **2021,** *52*, 223-35.[DOI: 10.1007/s11663-020-01991-w]

48. Xu, Y. B.; Yu, Y. M.; Liu, X. H.; Wang, G. D. Computer model of phase transformation from hot-deformed austenite in niobium microalloyed steels. *Journal of Iron and Steel Research International* **2007,** *14*, 66-69.[DOI: 10.1016/S1006-706x(07)60030-2]

49. Cahn, J. W. The kinetics of grain boundary nucleated reactions. *Acta Metallurgica* **1956,** *4*, 449-59.[DOI: 10.1016/0001-6160(56)90041-4]

50. Pohjonen, A.; Somani, M.; Porter, D. Effects of chemical composition and austenite deformation on the onset of ferrite formation for arbitrary cooling paths. *Metals* **2018,** *8*, 540.[DOI: 10.3390/met8070540]

51. Aranas, C.; Rodrigues, S.; Fall, A.; Jahazi, M.; Jonas, J. Determination of the critical stress associated with dynamic phase transformation in steels by means of free energy method. *Metals* **2018,** *8*, 360.[DOI: 10.3390/met8050360]

52. Dutta, T.; Dey, S.; Datta, S.; Das, D. Designing dual-phase steels with improved performance using ann and ga in tandem. *Computational Materials Science* **2019,** *157*, 6-16.[DOI: 10.1016/j.commatsci.2018.10.020]

53. Chang, Y.-J.; Jui, C.-Y.; Lee, W.-J.; Yeh, A.-C. Prediction of the composition and hardness of high-entropy alloys by machine learning: Chang, jui, lee, and yeh. *Jom* **2019,** *71*, 3433-42.[DOI: 10.1007/s11837-019-03704-4]

54. Zhao, Y. B.; Song, Y.; Li, F. F.; Yan, X. L. Prediction of mechanical properties of cold rolled strip based on improved extreme random tree. *Journal of Iron and Steel Research International* **2023,** *30*, 293-304.[DOI: 10.1007/s42243-022-00815-2]

55. Millner, G.; Mücke, M.; Romaner, L.; Scheiber, D. Machine learning mechanical properties of steel sheets from an industrial production route. *Materialia* **2023,** *30*, 101810.[DOI: 10.1016/j.mtla.2023.101810]

56. Jeon, J.; Sung, Y.; Seo, N.; Jung, J. G.; Son, S. B.; Lee, S. J. Machine learning model and prediction mechanisms of bainite start temperature of low alloy steels.

Materials Transactions **2023,** *64*, 2214-8.[DOI: 10.2320/matertrans.MT-MI2022007]

57. Zhang, Y.; Cheng, L.; Pan, A.; Hu, C.; Wu, K. Phase transformation temperature prediction in steels via machine learning. *Materials (Basel)* **2024,** *17*, 1117.[DOI: 10.3390/ma17051117]

58. Jeon, J.; Seo, N.; Jung, J. G.; Son, S. B.; Lee, S. J. Analysis of prediction mechanisms and feature importance of martensite start temperature of alloy steel via explainable artificial intelligence. *Materials Transactions* **2023,** *64*, 2196-201.[DOI: 10.2320/matertrans.MT-MI2022004]

59. Li, X. C.; Zheng, M. J.; Yang, X. Y.; Chen, P. H.; Ding, W. Y. A property-oriented design strategy of high-strength ductile rafm steels based on machine learning. *Materials Science and Engineering a-Structural Materials Properties Microstructure and Processing* **2022,** *840*, 142891.[DOI: 10.1016/j.msea.2022.142891]

60. Trzaska, J.; Sitek, W. A hybrid method for calculating the chemical composition of steel with the required hardness after cooling from the austenitizing temperature. *Materials (Basel)* **2023,** *17*, 97.[DOI: 10.3390/ma17010097]

61. Kaplan, A.; Haenlein, M. Siri, siri, in my hand: Who's the fairest in the land? On the interpretations, illustrations, and implications of artificial intelligence. *Business Horizons* **2019,** *62*, 15-25.[DOI: 10.1016/j.bushor.2018.08.004]

62. Ramprasad, R.; Batra, R.; Pilania, G.; Mannodi-Kanakkithodi, A.; Kim, C. Machine learning in materials informatics: Recent applications and prospects. *Npj Computational Materials* **2017,** *3*, 1-13.[DOI: 10.1038/s41524-017-0056-5]

63. Durodola, J. F. Machine learning for design, phase transformation and mechanical properties of alloys. *Progress in Materials Science* **2022,** *123*, 100797.[DOI: 10.1016/j.pmatsci.2021.100797]

64. L'Heureux, A.; Grolinger, K.; Elyamany, H. F.; Capretz, M. A. M. Machine learning with big data: Challenges and approaches. *Ieee Access* **2017,** *5*, 7776-97.[DOI: 10.1109/Access.2017.2696365]

65. Zhou, L. N.; Pan, S. M.; Wang, J. W.; Vasilakos, A. V. Machine learning on big data: Opportunities and challenges. *Neurocomputing* **2017,** *237*, 350-61.[DOI: 10.1016/j.neucom.2017.01.026]

66. Shiraiwa, T.; Miyazawa, Y.; Enoki, M. Prediction of fatigue strength in steels by linear regression and neural network. *Materials Transactions* **2019,** *60*, 189-98.[DOI: 10.2320/matertrans.ME201714]

67. Zhao, Z.; Yong, X.; Liu, S.; Zhou, M.; IEEE Data-driven surplus material prediction in steel coil production. In *2020 29TH WIRELESS AND OPTICAL COMMUNICATIONS CONFERENCE (WOCC)*, 2020-01-01; 2020; pp 1-6.[DOI: 10.1109/wocc48579.2020.9114917]

68. Yazici, C.; Domínguez-Gutiérrez, F. J. Machine learning techniques for estimating high-temperature mechanical behavior of high strength steels. *Results in Engineering* **2025,** *25*, 104242.[DOI: 10.1016/j.rineng.2025.104242]

69. Kavya, B. R.; Shrikanth, A. S.; Sreekeshava, K. S. Prediction of shear strength of steel fiber-reinforced concrete beams with stirrups using hybrid machine learning and deep learning models. *Buildings* **2025,** *15*, 1265.[DOI: 10.3390/buildings15081265]

70. Dong, G. B.; Li, X. C.; Zhao, J. X.; et al. Machine learning guided methods in building chemical composition- hardenability model for wear-resistant steel. *Materials Today Communications* **2020,** *24*, 101332.[DOI: 10.1016/j.mtcomm.2020.101332]

71. Hnatik, J.; Fulemova, J.; Sklenicka, J.; et al. Comprehensive experimental analysis of the effect of drilled material on torque using machine learning decision trees. *Materials (Basel)* **2025,** *18*, 3145.[DOI: 10.3390/ma18133145]

72. Geng, X.; Wang, S.; Ullah, A.; Wu, G.; Wang, H. Prediction of hardenability curves for non-boron steels via a combined machine learning model. *Materials (Basel)* **2022,** *15*, 3127.[DOI: 10.3390/ma15093127]

73. Paz da Silva, F.; Matos, R. S.; da Fonseca Filho, H. D.; et al. Non-destructive ultrasonic testing and machine learning-assisted early detection of carburizing damage in hp steel pyrolysis furnace tubes. *Measurement* **2023,** *218*, 113221.[DOI: 10.1016/j.measurement.2023.113221]

74. Ramachandran, R. Machine learning model to map tribocorrosion regimes in feature space. *Coatings* **2021,** *11*, 450.[DOI: 10.3390/coatings11040450]

75. Cohn, R.; Holm, E. Unsupervised machine learning via transfer learning and k-means clustering to classify materials image data. *Integrating Materials and*

Manufacturing Innovation **2021,** *10*, 231-44.[DOI: 10.1007/s40192-021-00205-8]

76. Niu, T. J.; Lee, R. S.; Lam, S.; et al. A novel machine learning-driven approach to high throughput mechanical testing. *Jom* **2025,** *77*, 2121-33.[DOI: 10.1007/s11837-024-07063-7]

77. Wiessner, M.; Gamsjäger, E. Characterization of high-speed steels-experimental data and their evaluation supported by machine learning algorithms. *Metals* **2025,** *15*, 194.[DOI: 10.3390/met15020194]

78. Li, W. X.; He, Y. X.; Li, Y.; Cai, F. N.; Zhang, Y. Rapid identification of homogeneous alloys based on laser-induced breakdown spectroscopy combined with machine-learning algorithms. *Laser & Optoelectronics Progress* **2024,** *61*, 1730001.[DOI: 10.3788/Lop232417]

79. Wen, C.; Zhang, Y.; Wang, C. X.; et al. Machine learning assisted design of high entropy alloys with desired property. *Acta Mater* **2019,** *170*, 109-17.[DOI: 10.1016/j.actamat.2019.03.010]

80. Hu, M. W.; Tan, Q. Y.; Knibbe, R.; et al. Recent applications of machine learning in alloy design: A review. *Materials Science & Engineering R-Reports* **2023,** *155*, 100746.[DOI: 10.1016/j.mser.2023.100746]

81. Pan, G. F.; Wang, F. Y.; Shang, C. L.; et al. Advances in machine learning- and artificial intelligence-assisted material design of steels. *International Journal of Minerals Metallurgy and Materials* **2023,** *30*, 1003-24.[DOI: 10.1007/s12613-022-2595-0]

82. Shen, C. G.; Wang, C. C.; Wei, X. L.; Li, Y.; van der Zwaag, S.; Xu, W. Physical metallurgy-guided machine learning and artificial intelligent design of ultrahigh-strength stainless steel. *Acta Mater* **2019,** *179*, 201-14.[DOI: 10.1016/j.actamat.2019.08.033]

83. Wei, X. L.; van der Zwaag, S.; Jia, Z. X.; Wang, C. C.; Xu, W. On the use of transfer modeling to design new steels with excellent rotating bending fatigue resistance even in the case of very small calibration datasets. *Acta Mater* **2022,** *235*, 118103.[DOI: 10.1016/j.actamat.2022.118103]

84. Liu, Y.; Sun, J. B.; Liu, S. J.; Liu, Z. A.; Yin, F. X. Optimization of ultra-high and

high manganese steel based on artificial neural network and genetic algorithm. *Journal of Materials Engineering and Performance* **2023,** *32*, 9864-74.[DOI: 10.1007/s11665-023-07827-3]

85. Hu, X. B.; Chen, Y. M.; Lu, J. L.; et al. Three-step learning strategy for designing 15cr ferritic steels with enhanced strength and plasticity at elevated temperature. *Journal of Materials Science & Technology* **2023,** *164*, 79-94.[DOI: 10.1016/j.jmst.2023.04.034]

86. Guo, Z.; Sha, W.; Wilson, E. A. Modeling the evolution of microstructure during the processing of maraging steels. *Jom* **2004,** *56*, 62-6.[DOI: 10.1007/s11837-004-0037-2]

87. Geng, X. X.; Cheng, Z.; Wang, S. Z.; et al. A data-driven machine learning approach to predict the hardenability curve of boron steels and assist alloy design. *Journal of Materials Science* **2022,** *57*, 10755-68.[DOI: 10.1007/s10853-022-07132-9]

88. Murdoch, H. A.; Field, D. M.; Szajewski, B. A.; et al. Tempered hardness optimization of martensitic alloy steels. *Integrating Materials and Manufacturing Innovation* **2023,** *12*, 301-20.[DOI: 10.1007/s40192-023-00311-9]

89. Jeon, J.; Seo, N.; Son, S. B.; Lee, S. J.; Jung, M. Application of machine learning algorithms and shap for prediction and feature analysis of tempered martensite hardness in low-alloy steels. *Metals* **2021,** *11*, 1159.[DOI: 10.3390/met11081159]

90. Dobrzanski, L. A.; Trzaska, J. Application of neural networks for the prediction of continuous cooling transformation diagrams. *Computational Materials Science* **2004,** *30*, 251-9.[DOI: 10.1016/j.commatsci.2004.02.011]

91. Chakraborty, S.; Chattopadhyay, P. P.; Ghosh, S. K.; Datta, S. Incorporation of prior knowledge in neural network model for continuous cooling of steel using genetic algorithm. *Applied Soft Computing* **2017,** *58*, 297-306.[DOI: 10.1016/j.asoc.2017.05.001]

92. Trzaska, J. A new neural networks model for calculating the continuous cooling transformation diagrams. *Archives of Metallurgy and Materials* **2018,** *63*, 2009-15.[DOI: 10.24425/amm.2018.125137]

93. Chakraborty, S.; Das, P.; Kaveti, N. K.; Chattopadhyay, P. P.; Datta, S. Mcdm towards knowledge incorporation in ann models for phase transformation in continuous

cooling of steel. *Multidiscipline Modeling in Materials and Structures* **2019,** *15*, 170-86.[DOI: 10.1108/Mmms-01-2018-0002]

94. Minamoto, S.; Tsukamoto, S.; Kasuya, T.; Watanabe, M.; Demura, M. Prediction of continuous cooling transformation diagram for weld heat affected zone by machine learning. *Science and Technology of Advanced Materials: Methods* **2022,** *2*, 402-15.[DOI: 10.1080/27660400.2022.2123262]

95. Geng, X. X.; Mao, X. P.; Wu, H. H.; *et al.* A hybrid machine learning model for predicting continuous cooling transformation diagrams in welding heat-affected zone of low alloy steels. *Journal of Materials Science & Technology* **2022,** *107*, 207-15.[DOI: 10.1016/j.jmst.2021.07.038]

96. Huang, X. Y.; Zhang, B.; Tian, Q.; et al. Machine learning study on time-temperature-transformation diagram of carbon and low-alloy steel. *Journal of Iron and Steel Research International* **2023,** *30*, 1032-41.[DOI: 10.1007/s42243-023-00932-6]

97. Geng, X. X.; Wang, H.; Ullah, A.; et al. Prediction of continuous cooling transformation diagrams for ni-cr-mo welding steels via machine learning approaches. *Jom* **2020,** *72*, 3926-34.[DOI: 10.1007/s11837-020-04057-z]

98. Zhang, B.; Wang, B. G.; Xue, W. H.; Ullah, A.; Zhang, T. H.; Wang, H. Development of a machine learning model for prediction of continuous cooling transformation diagrams in welding heat-affected zone. *Journal of Materials Science* **2023,** *58*, 4795-808.[DOI: 10.1007/s10853-023-08322-9]

99. Rahaman, M.; Mu, W. Z.; Odqvist, J.; Hedström, P. Machine learning to predict the martensite start temperature in steels. *Metallurgical and Materials Transactions a-Physical Metallurgy and Materials Science* **2019,** *50a*, 2081-91.[DOI: 10.1007/s11661-019-05170-8]

100. Mandal, G.; Ghosh, S. K.; Mukherjee, S. Phase transformation and mechanical behaviour of thermo-mechanically controlled processed high-strength multiphase steel. *Journal of Materials Science* **2016,** *51*, 6569-82.[DOI: 10.1007/s10853-016-9852-4]

101. Krbata, M.; Krizan, D.; Eckert, M.; Kaar, S.; Dubec, A.; Ciger, R. Austenite decomposition of a lean medium mn steel suitable for quenching and partitioning

process: Comparison of cct and dcct diagram and their microstructural changes. *Materials (Basel)* **2022,** *15*, 1753.[DOI: 10.3390/ma15051753]

102. Schindler, I.; Kawulok, R.; Seillier, Y.; et al. Continuous cooling transformation diagrams of hsla steel for seamless tubes production. *Journal of Mining and Metallurgy Section B-Metallurgy* **2019,** *55*, 413-26.[DOI: 10.2298/Jmmb181217031s]

103. Kawulok, P.; Podolinsky, P.; Kajzar, P.; et al. The influence of deformation and austenitization temperature on the kinetics of phase transformations during cooling of high-carbon steel. *Archives of Metallurgy and Materials* **2018,** *63*, 1743-8.[DOI: 10.24425/amm.2018.125100]

104. Bao, J.; Ma, J.; Zhao, J.; Ning, B. Transformation behavior of austenite continuous cooling of nb-ti micro-alloyed low carbon steel. In *ADVANCES IN MATERIALS AND MATERIALS PROCESSING, PTS 1-3*, 2013-01-01; 2013; Vol. 652-4, pp 967-970.[DOI: 10.4028/www.scientific.net/AMR.652-654.967]

105. Wei, H.; Chen, Y. L.; Su, L.; Tang, D. Effect of simulated thermomechanical processing on transformation behavior and microstructure of 82b steel. *Journal of Iron and Steel Research International* **2019,** *26*, 69-77.[DOI: 10.1007/s42243-018-0209-x]

106. Zhou, X.; Li, H.; Chen, Q.; Liu, Z. Controlled rolling of x80 pipeline steel in the austenite recrystallization temperature region and its effect on the microstructure and mechanical properties. *steel research international* **2021,** *93*, 2100331.[DOI: 10.1002/srin.202100331]

107. Kawulok, R.; Schindler, I.; Sojka, J.; et al. Effect of strain on transformation diagrams of 100cr6 steel. *Crystals* **2020,** *10*, 326.[DOI: 10.3390/cryst10040326]

108. Cao, G. M.; Gao, Z. W.; Gao, X. Y. Predicting flow stress of ni steel based on machine learning algorithm. *Proceedings of the Institution of Mechanical Engineers Part C-Journal of Mechanical Engineering Science* **2022,** *236*, 4253-66.[DOI: 10.1177/09544062211048175]

109. Zener, C.; Hollomon, J. H. Effect of strain rate upon plastic flow of steel. *Journal of Applied Physics* **1944,** *15*, 22-32.[DOI: 10.1063/1.1707363]

110. Dehghan, H.; Rezayat, M.; Ebrahimi, S. A. S. Modeling of strain induced transformation during hot deformation of an mn-al-c alloy. *Materials Science and*

Engineering a-Structural Materials Properties Microstructure and Processing **2020,** *776*, 139006.[DOI: 10.1016/j.msea.2020.139006]

111. Eckert, M.; Krbata, M.; Barenyi, I.; Majerik, J.; Dubec, A.; Bokes, M. Effect of selected cooling and deformation parameters on the structure and properties of aisi 4340 steel. *Materials (Basel)* **2020,** *13*, 5585.[DOI: 10.3390/ma13235585]

112. Medina, S. F.; Hernandez, C. A. General expression of the zener-hollomon parameter as a function of the chemical composition of low alloy and microalloyed steels. *Acta Mater* **1996,** *44*, 137-148.[DOI: 10.1016/1359-6454(95)00151-0]

113. Bengochea, R.; Lopez, B.; Gutierrez, I. Microstructural evolution during the austenite-to-ferrite transformation from deformed austenite. *Metallurgical and Materials Transactions a-Physical Metallurgy and Materials Science* **1998,** *29*, 417-26.[DOI: 10.1007/s11661-998-0122-1]

114. Li, Y. F.; Chen, Y.; Li, S. H. Phase transformation testing and modeling for hot stamping of boron steel considering the effect of the prior austenite deformation. *Materials Science and Engineering a-Structural Materials Properties Microstructure and Processing* **2021,** *821*, 141447.[DOI: 10.1016/j.msea.2021.141447]

115. Li, H. Y.; Wang, X. J.; Song, Y. H.; Li, Y. G.; Li, X.; Ji, Y. F. Physical metallurgy guided machine learning to predict hot deformation mechanism of stainless steel. *Materials Today Communications* **2023,** *36*, 106779.[DOI: 10.1016/j.mtcomm.2023.106779]

116. Cao, G. M.; Liu, Z. Y.; Cui, C. Y.; et al. Physical metallurgy guided deep learning for yield strength of hot-rolled steel based on the small labeled dataset. *Materials & Design* **2022,** *223*, 111269.[DOI: 10.1016/j.matdes.2022.111269]

117. Li, H. W.; Li, Y.; Huang, J.; et al. Physical metallurgy guided industrial big data analysis system with data classification and property prediction. *Steel Research International* **2022,** *93*, 2100820.[DOI: 10.1002/srin.202100820]

118. Xu, L. T.; Xu, Y. W.; Yang, G. W. Directly predicting hot ductility of steels using machine learning approaches. *Metallurgical and Materials Transactions a-Physical Metallurgy and Materials Science* **2025,** *56*, 5597-608.[DOI: 10.1007/s11661-025-07994-z]

119. Li, D. Z.; Yan, Z. J.; Wang, R.; Kang, Y.; Shen, L. Y. Effect of hot-deformation processes on phase transformation of low-alloyed, multiphase, high-strength steel. *Steel Research International* **2021,** *92*, 1900522.[DOI: 10.1002/srin.201900522]

120. Hanzaki, A. Z.; Pandi, R.; Hodgson, P. D.; Yue, S. Continous cooling deformation testing of steels. *Metallurgical Transactions a-Physical Metallurgy and Materials Science* **1993,** *24*, 2657-65.[DOI: 10.1007/Bf02666271]

121. Li, Z. A.; Wu, D.; Lv, H. S.; Fang, S. R. Continuous cooling transformation behaviour of c-si-mn trip steel. *Journal of Iron and Steel Research International* **2007,** *14*, 277-81.[DOI: 10.1016/S1006-706x(08)60094-1]

122. Kawulok, R.; Schindler, I.; Kawulok, P.; et al. Transformation kinetics of selected steel grades after plastic deformation. *Metalurgija* **2016,** *55*, 357-60.[DOI: 10.13140/RG.2.1.1401.0001]

123. Kawulok, R.; Schindler, I.; Kawulok, P.; et al. Effect of deformation on the continuous cooling transformation (cct) diagram of steel 32crb4. *Metalurgija* **2015,** *54*, 473-6.http://hdl.handle.net/10084/106418

124. Opiela, M.; Zalecki, W.; Grajcar, A. Influence of plastic deformation on cct-diagrams of new-developed microalloyed steel. *Journal of Achievements in Materials and Manufacturing Engineering* **2012,** *51*, 78-89.http://journalamme.org

125. Schindler, I.; Kawulok, R.; Opela, P.; et al. Effects of austenitization temperature and pre-deformation on cct diagrams of 23mnnicrmo5-3 steel. *Materials (Basel)* **2020,** *13*, 5116.[DOI: 10.3390/ma13225116]

126. Morawiec, M.; Skowronek, A.; Krol, M.; Grajcar, A. Dilatometric analysis of the austenite decomposition in undeformed and deformed low-carbon structural steel. *Materials (Basel)* **2020,** *13*, 5443.[DOI: 10.3390/ma13235443]

127. Grajcar, A.; Opiela, M. Influence of plastic deformation on cct-diagrams of low-carbon and medium-carbon trip-steels. *Journal of Achievements in Materials and Manufacturing Engineering* **2008,** *29*, 71-8.http://journalamme.org

128. Barcellona, A.; Palmeri, D. Effect of plastic hot deformation on the hardness and continuous cooling transformations of 22mnb5 microalloyed boron steel. *Metallurgical and Materials Transactions a-Physical Metallurgy and Materials Science* **2009,** *40a*,

1160-74.[DOI: 10.1007/s11661-009-9790-8]

129. Jun, H. J.; Kang, J. S.; Seo, D. H.; Kang, K. B.; Park, C. G. Effects of deformation and boron on microstructure and continuous cooling transformation in low carbon hsla steels. *Materials Science and Engineering a-Structural Materials Properties Microstructure and Processing* **2006,** *422*, 157-62.[DOI: 10.1016/j.msea.2005.05.008]]

130. Zhao, M. C.; Yang, K.; Xiao, F. R.; Shan, Y. Y. Continuous cooling transformation of undeformed and deformed low carbon pipeline steels. *Materials Science and Engineering a-Structural Materials Properties Microstructure and Processing* **2003,** *355*, 126-36.[DOI: 10.1016/S0921-5093(03)00074-1]

131. Katz, B.; Shaked, N. T.; Rosen, J. Synthesizing computer generated holograms with reduced number of perspective projections. *Opt Express* **2007,** *15*, 13250-5.[DOI: 10.1364/oe.15.013250]

132. Li, Y.; He, Y.; Liu, J.; *et al.* Effects of austenite deformation on continuous cooling transformation of the pearlite heat-resistant steel. *Ironmaking & Steelmaking* **2020,** *48*, 402-8.[DOI: 10.1080/03019233.2020.1799699]

133. Xiao, F. R.; Liao, B.; Qiao, G. Y.; Guan, S. Z. Effect of hot deformation on phase transformation kinetics of 86crmov7 steel. *Materials Characterization* **2006,** *57*, 306-13.[DOI: 10.1016/j.matchar.2006.02.003]

134. Nikravesh, M.; Naderi, M.; Akbari, G. H.; Bleck, W. Phase transformations in a simulated hot stamping process of the boron bearing steel. *Materials & Design* **2015,** *84*, 18-24.[DOI: 10.1016/j.matdes.2015.06.108]

135. Kawulok, R.; Kawulok, P.; Schindler, I.; et al. Study of the effect of deformation on transformation diagrams of two low-alloy manganese-chromium steels. *Archives of Metallurgy and Materials* **2018,** *63*, 1735-41.[DOI: 10.24425/amm.2018.125099]

136. Freiwillig, R.; Kudrman, J.; Chraska, P. Bainite transformation in deformed austenite. *Metallurgical Transactions a-Physical Metallurgy and Materials Science* **1976,** *7*, 1091-7.[DOI: 10.1007/Bf02656591]